

Article

Mineralogical Evidence for Partial Melting and Melt-Rock Interaction Processes in the Mantle Peridotites of Edessa Ophiolite (North Greece)

Aikaterini Rogkala ^{1,*}, Petros Petrounias ¹, Basilios Tsikouras ²,
Panagiota P. Giannakopoulou ¹ and Konstantin Hatzipanagiotou ¹

¹ Section of Earth Materials, Department of Geology, University of Patras, 265 04 Patras, Greece; Geo.plan@outlook.com (P.P.); peny_giannakopoulou@windowslive.com (P.P.G.); k.hatzipanagiotou@upatras.gr (K.H.)

² Physical and Geological Sciences, Faculty of Science, Universiti Brunei Darussalam, Jalan Tungku Link, Gadong BE1410, Bandar Seri Begawan, Brunei Darussalam; basilios.tsikouras@ubd.edu.bn

* Correspondence: krogkala@upatras.gr; Tel.: +30-2610996288

Received: 10 December 2018; Accepted: 14 February 2019; Published: 17 February 2019



Abstract: The Edessa ophiolite complex of northern Greece consists of remnants of oceanic lithosphere emplaced during the Upper Jurassic-Lower Cretaceous onto the Palaeozoic-Mesozoic continental margin of Eurasia. This study presents new data on mineral compositions of mantle peridotites from this ophiolite, especially serpentinised harzburgite and minor lherzolite. Lherzolite formed by low to moderate degrees of partial melting and subsequent melt-rock reaction in an oceanic spreading setting. On the other hand, refractory harzburgite formed by high degrees of partial melting in a supra-subduction zone (SSZ) setting. These SSZ mantle peridotites contain Cr-rich spinel residual after partial melting of more fertile (abyssal) lherzolite with Al-rich spinel. Chromite with Cr# > 60 in harzburgite resulted from chemical modification of residual Cr-spinel and, along with the presence of euhedral chromite, is indicative of late melt-peridotite interaction in the mantle wedge. Mineral compositions suggest that the Edessa oceanic mantle evolved from a typical mid-ocean ridge (MOR) oceanic basin to the mantle wedge of a SSZ. This scenario explains the higher degrees of partial melting recorded in harzburgite, as well as the overprint of primary mineralogical characteristics in the Edessa peridotites.

Keywords: Edessa ophiolite; harzburgite; Al-spinel; Cr-spinel; chromite; SSZ peridotites

1. Introduction

Ophiolites are fragments of oceanic lithosphere that have been emplaced tectonically along continental margins in accretionary prisms during orogenic processes. They may be intact and almost complete or have an incomplete stratigraphy and frequently they are tectonically underlain by an ophiolitic mélangé. Ophiolites provide important information for the evolution of ancient oceanic crust and mantle beneath spreading centers in mid-ocean ridge (MOR) and supra-subduction zone (SSZ) tectonic settings [1–5]. Subduction-related and subduction-unrelated ophiolites form in a variety of tectonic settings [6]. The chemical composition of ophiolitic rocks is commonly used for recognising a variety of different tectonic settings, as well as the nature of mantle sources. These tectonic settings include oceanic spreading centers, hot spots, backarc and forearc basins (supra-subduction zone environments), arcs and other extensional magmatic settings including those in association with plumes [3,7–12]. Furthermore, they provide information about magmatic, metamorphic and tectonic processes of the oceanic crust and upper mantle [3,13,14]. Mantle rocks of ophiolitic origin provide significant information for the paleotectonic evolution of the oceanic

lithosphere, partial melting, melt-rock interaction and mantle melt fractionation [15–19]. Specifically, the abyssal peridotites represent mantle residues produced by partial melting beneath MOR whereas the highly depleted SSZ-type peridotites represent mantle rocks that have experienced intense melting above a subduction zone.

Serpentinisation is a common secondary process in these lithologies that can take place in both mid-ocean ridge and subduction zones and can strongly affect their primary mineralogical composition, thus obscuring any primary data that can provide petrogenetic information, as well to degrade their quality for several industrial applications [20–23]. Spinel-group minerals have a wide range of compositions reflecting a residual or secondary origin and are normally resistant to serpentinisation, thus they are commonly used as petrogenetic and geotectonic indicators. Their chemical composition depends on the petrogenesis (crystallisation from melt, residue after partial melting) and physical conditions (temperature, pressure, oxygen fugacity) of their host peridotites [24–31]. Additionally, the degree of partial melting can be calculated using the chemical composition of unaltered spinel-group minerals.

Ophiolitic rocks occur along two subparallel zones in Greece, the western (or external) and the eastern (or internal), which are thought to represent the sutures of Pindos and Axios (or Vardar) Oceans, respectively (although several authors argue for one ocean), which have been formed during progressive opening and closure of the Mesozoic Neo-Tethyan Oceanic domain (Figure 1). The ophiolitic complex of Edessa, in the internal zone, comprises a series of oceanic crust and mantle fragments linking the Veria-Naousa and Vermion ophiolite suites (to the S) to the Guevgeuli ophiolite (to the NE) (Figure 1). Despite the geological significance of the Edessa ophiolitic complex, few available comprehensive data on the geology and petrology of these rocks have been reported [10,32,33].

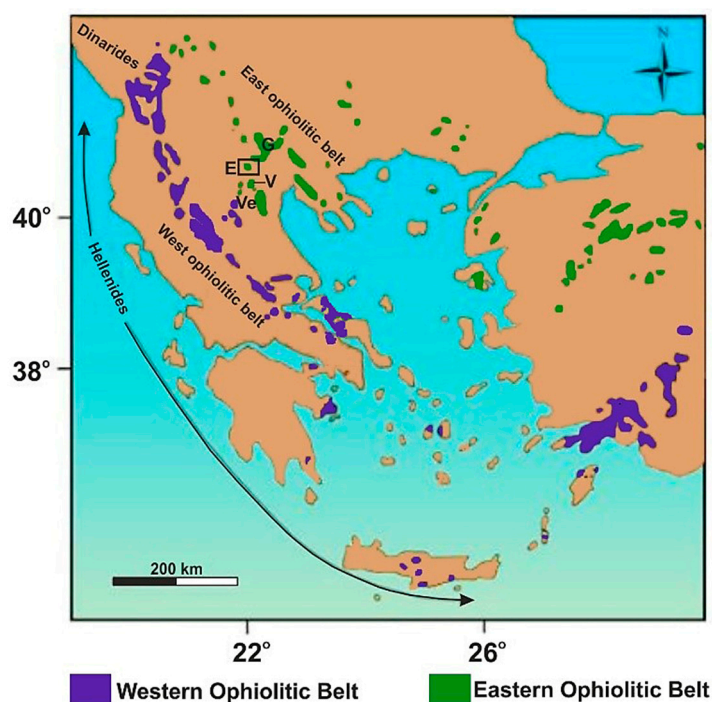


Figure 1. Distribution of ophiolites in the southernmost part of the Balkan Peninsula and Turkey (modified after Végely [34]). Key to lettering: E = Edessa (also marked by the open square), G: Guevgeuli, V: Veria-Naousa, Ve: Vermion.

The aim of the present paper is to provide new data including field observations, mineral chemistry and specifically the chemical variability of spinel-group minerals of ultramafic rocks from the Edessa ophiolite complex, in order to shed more light into their petrogenesis and their tectonic setting.

2. Geological Setting

The Edessa ophiolite represents remnants of an oceanic lithosphere obducted onto Palaeozoic-Mesozoic marbles and schists during Upper Jurassic to Lower Cretaceous [33,35]. The ophiolitic rocks include several tectonic units that are considered to be the northwards continuation of the Veria-Naousa ophiolite [32,36,37].

An ophiolitic matrix *mélange* formation occurs tectonically beneath the ophiolite near Ekklisochori village. It comprises a multi-coloured heterogeneous formation with a chaotic internal structure that consists of tectonic blocks of serpentinites, basalts, marbles and schists surrounded by a tectonised, serpentinitic matrix. It is structurally overlain by a local sub-ophiolitic metamorphic sole, composed of amphibolites and both formations are overthrust by upper mantle tectonites (Figure 2). These rocks at the lower part of the Edessa ophiolite comprise serpentinitised harzburgite and minor lherzolite overlain by diorite, gabbro, diabase and basalt (Figure 2). The serpentinitised harzburgite displays dark green colour and local relic pyroxenes with moderate to intense mantle deformation features, such as banding and foliation. Locally, it encloses lenses, pods or elongated bodies (up to few meters) of chromitite, which according to their texture and mode of occurrence, are classified as massive and disseminated podiform bodies. Small-scale irregular joints are also developed in the rocks with the presence of slickensides and striations. Moderately serpentinitised lherzolite is an infrequent, medium grained rock, which is characterised by greenish black to dark green colour and conchoidal fracture. It occurs as relic, irregular bodies up to a few meters, surrounded by harzburgite (Figure 3a,b). Local lherzolite slivers are repeated in the mantle domain of Edessa due to a series of imbricated thrusts occurring through the area. Light to dark green veins of dunite (up to few cm thick) locally penetrate the lherzolite (Figure 3b).

Sparse gabbroic and dioritic dykes intrude the serpentinitised harzburgite. The medium to coarse-grained, pale green dykes display chilled margins and have a thickness of up to 10 m. Some of the gabbroic dykes are intensely rodingitised. Massive gabbros are rare in the Edessa ophiolite; only near the villages of Agia Foteini and Krania massive gabbro were observed in tectonic contact with serpentinitised harzburgite and diabase, respectively. Massive diabase and basalt are thrust over serpentinitised harzburgite and pass upwards into basaltic pillow-lava flows. The diabase is usually dark green and locally shows low grade metamorphism characteristics. The thrust contacts of the massive diabase and the serpentinitised harzburgite form cataclastic zones.

The ophiolitic rocks are unconformably overlain by middle Upper Cretaceous to Palaeocene sedimentary formations (conglomeratic limestone, brecciated limestone) and Neogene to Quaternary deposits (alluvial sediments, talus, travertine) (Figure 2). The serpentinitised harzburgite is overthrust by flysch. Pliocene andesite and rhyolite have intruded the ophiolite (Figure 2). According to Sr–Nd isotopes, they are associated with a SSZ tectonic environment, in the Early Tertiary during the subduction of Africa beneath Eurasia [40].

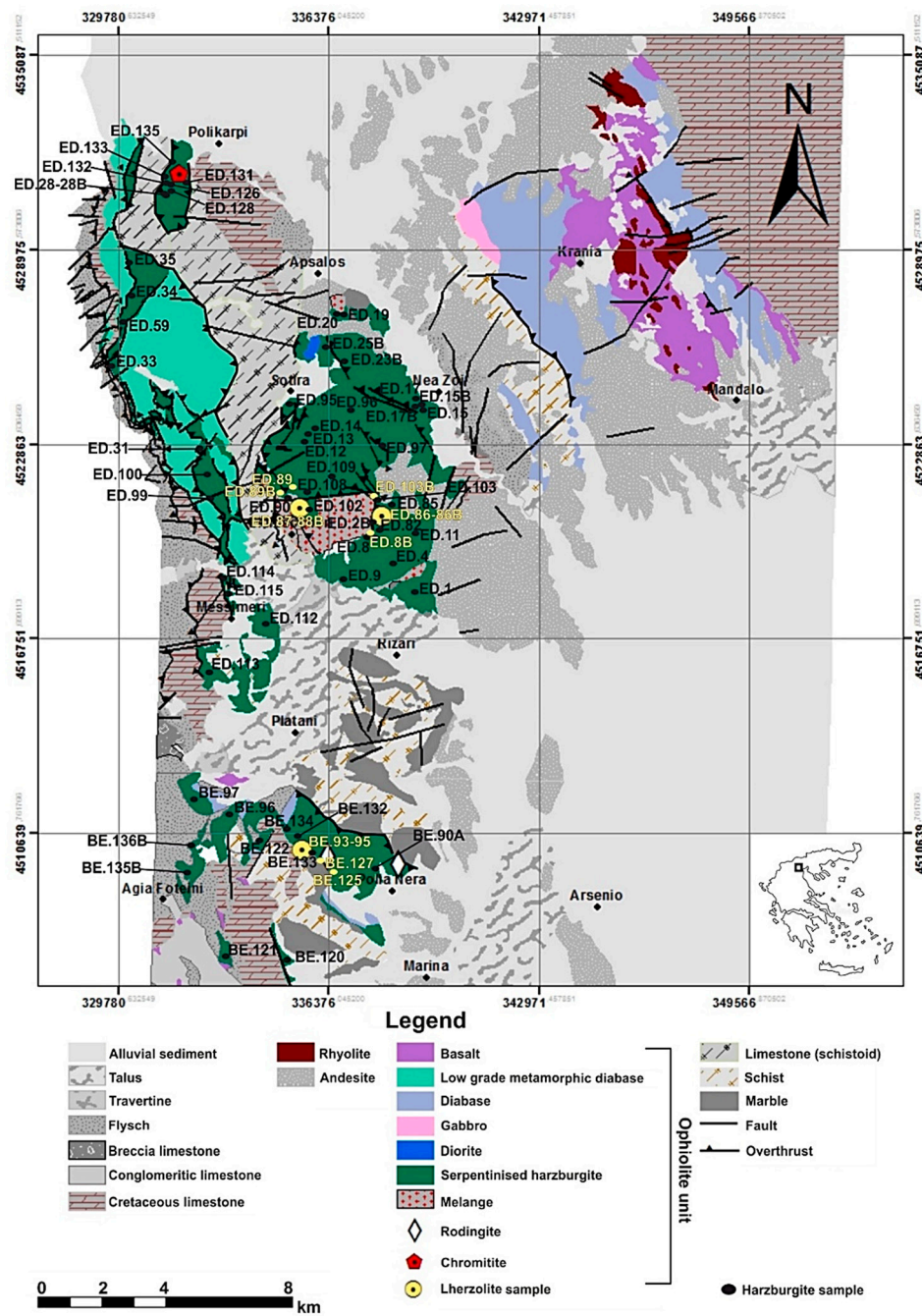


Figure 2. Geological and sampling map of the Edessa ophiolite (from IGME [38,39], modified after fieldwork and mapping by using ArcMap 10.1); rectangle in the inset shows the study area.



Figure 3. Views of the studied peridotite: (a) Irregular lherzolite body (~10 m) surrounded by serpentinised harzburgite; (b) dunite veins penetrate a lherzolite body.

3. Petrographic Features

3.1. Lherzolite

The petrographic description of the lherzolite was made in polished-thin sections from 15 fresh samples, which were collected throughout the whole exposure, thus reflecting all accessible localities. The lherzolite samples display mainly porphyroclastic texture (Figure 4a–d). Their primary mineralogical assemblage includes olivine (40–60 vol. %), orthopyroxene (30–40 vol. %), clinopyroxene (5–25 vol. %) and spinel (up to 5%).

Rare Fe–Ni–Co sulphides with Cu (pyrite, pentlandite and millerite) and ilmenite are associated to spinel. Olivine and orthopyroxenes show strain lamellae, kink bands, undulose extinction, shearing and recrystallisation, all typical features of plastic deformation of upper mantle peridotites (Figure 4a,c,d). Olivine displays porphyroclastic grains (up to 2 cm long) and smaller neoblasts (Figure 4a,b). Orthopyroxene porphyroclasts (up to 3 cm long) are elongated and exhibit exsolution lamellae of clinopyroxene (Figure 4c). Olivine and orthopyroxene porphyroclasts are surrounded and partly replaced by neoblastic olivine (Figure 4b,c). The clinopyroxene occurs as porphyroclastic (0.5–1 cm long Figure 4a,b) and neoblastic grains in the recrystallised matrix. Spinel is of aluminous composition and forms anhedral to subhedral grains with lobate boundaries (Figure 4d,e). This Al-spinel is locally replaced by veins and rims of garnet, which is a solid solution dominated hydrogrossular and hydroandradite molecules (Figure 4e). The Al-spinel often displays thin rims of secondary magnetite. Local, fine-grained, euhedral Cr-spinel occurring along the cleavage of orthopyroxene porphyroclasts is thought to be of secondary origin (Figure 4e). Secondary phases also include serpentine, chlorite, tremolite and magnetite. Dunite veins (up to a few cm thick) occur in some lherzolitic samples with less deformed segregations of olivine penetrating the porphyroclastic lherzolite, as an indication of melt percolation.

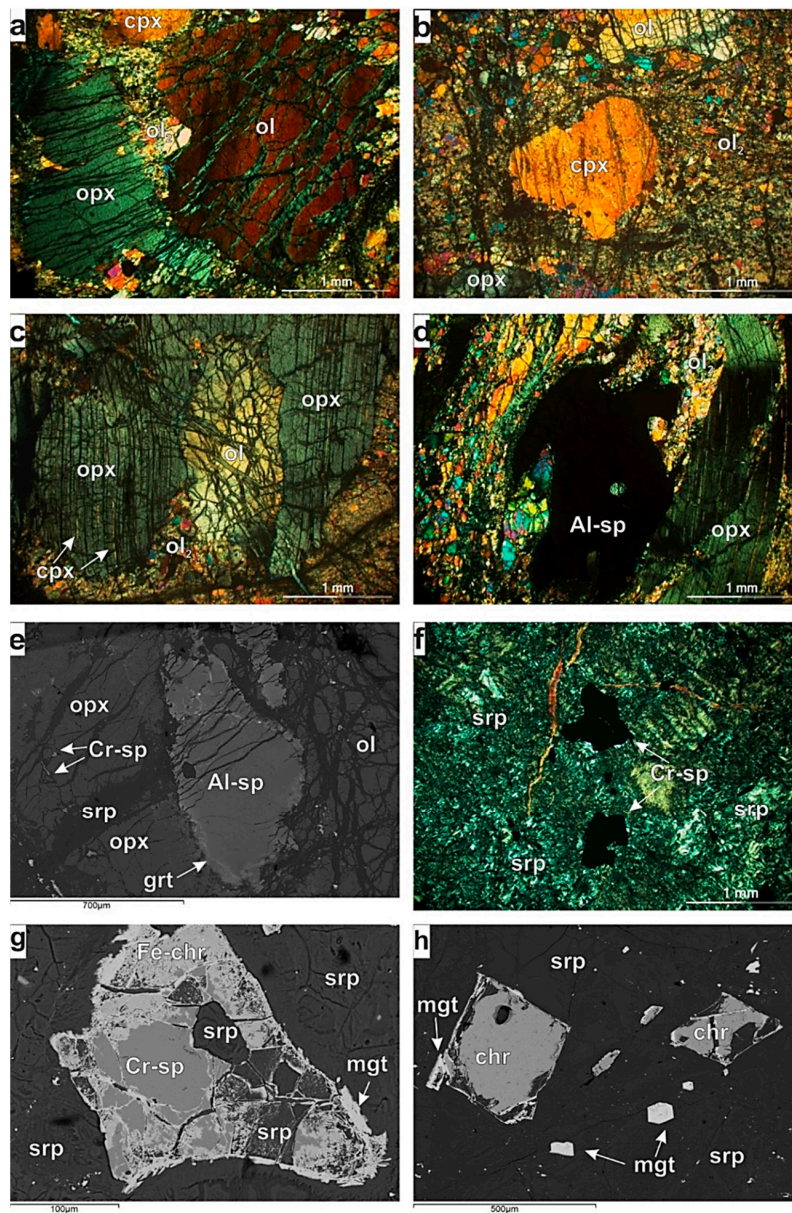


Figure 4. Textural characteristics of ultramafic rocks from Edessa ophiolite: (a) Photomicrograph of porphyroclastic texture in a lherzolite, showing porphyroclasts of orthopyroxene (opx) olivine (ol) and clinopyroxene (cpx) surrounded and partially replaced by neoblastic olivine (ol₂) (sample ED.88, + Nicols); (b) Photomicrograph of strained clinopyroxene (cpx), olivine (ol) and orthopyroxene (opx) porphyroclasts in a lherzolite surrounded by neoblastic olivine (ol₂) (sample ED.86, + Nicols); (c) Photomicrograph of an orthopyroxene (opx) porphyroclast with exsolution lamellae of clinopyroxene (cpx) replaced and surrounded by olivine neoblasts (ol₂) in a lherzolite (sample ED.86, + Nicols); (d) Photomicrograph of anhedral Al-spinel (Al-sp) with lobate boundaries and banded orthopyroxene porphyroclast (opx) surrounded by olivine neoblasts (ol₂) in a lherzolite (sample ED.87, + Nicols); (e) Back-scattered electron image of anhedral Al-spinel (Al-sp) rimmed by garnet (grt), and surrounded by olivine (ol) and orthopyroxene (opx) porphyroclasts in a lherzolite. Secondary Cr-spinel (Cr-sp) is developed along the cleavage of partially serpentinised (srp) opx (sample ED.89); (f) Photomicrograph of interlocking and hourglass serpentine (srp) and anhedral Cr-spinel (Cr-sp) in a serpentinised harzburgite (sample ED.28.1, + Nicols); (g) Back-scattered electron image of Cr-spinel (Cr-sp) with curved boundaries and thick rims of ferritchromite (Fe-chr) and magnetite (mgt) in a serpentinised harzburgite (sample ED.28.2); (h) Back-scattered electron image of euhedral chromite (chr) with thin rims of magnetite (mgt) in serpentinised matrix (sample ED.115).

3.2. Serpentinised Harzburgite

Sixty harzburgite samples were collected, which are intensely serpentinised. The samples were collected in a way to represent a more or less equal distribution in the peridotite exposure, in order to identify potential variations throughout the peridotite outcrops. Their primary mineralogical assemblage constitutes less than 5% of the mode and comprises relics of clinopyroxene, Cr-spinel and chromite (Figure 4f). Clinopyroxene appears as remnants of subhedral porphyroclasts in few samples. Two types of spinels are observed in these samples and even in the same thin section: Cr-spinel crystals, which are anhedral to subhedral with curved and lobate boundaries (Figure 4f,g) and chromite crystals, which are euhedral and rarely subhedral (Figure 4h). The Cr-spinel shows thick rims of Cr-bearing magnetite and Mn-bearing ferritchromite whereas the chromite displays thin rims of Cr-bearing magnetite (Figure 4g,h). Serpentine is the main alteration product showing mesh, ribbon, bastite, hourglass and interlocking textures (Figure 4f). Chlorite and magnetite are also secondary products in the harzburgite. Locally, quartz replaces serpentine, thus suggesting an incipient stage of listwaenitisation.

4. Analytical Methods

The mineralogical and textural characteristics of the samples were studied in polished-thin sections in optical and scanning electron microscopes (SEM). Mineral microanalyses were performed using a JEOL JSM-6300 SEM equipped with energy dispersive and wavelength spectrometers (EDS and WDS) and INCA software at the Laboratory of Electron Microscopy and Microanalysis, University of Patras. Operating conditions were accelerating voltage 25 kV and beam current 3.3 nA, with a 4 µm beam diameter. The total counting time was 60 s and dead-time 40%. Synthetic oxides and natural minerals were used as standards for our analyses. Detection limits are ~0.1% and accuracy better than 5% was obtained.

5. Mineral Chemistry

5.1. Spinel-Group Minerals

Representative microanalyses of spinel-group minerals are reported in Table 1 and plotted in Figure 5. The analysed spinels plot in distinctive clusters on their Mg# vs. Cr# diagram (Figure 5) and with the aid of this and according to their Cr# [= $100 \times \text{Cr}/(\text{Cr} + \text{Al})$], they are classified into Al-spinel (Cr# < 30), Cr-spinel (Cr# = 30–60) and chromite (Cr# > 60).

Al-spinel crystals occur in the lherzolite and display Cr# values ranging from 7.5 to 28.6 and Mg# [= $100 \times \text{Mg}/(\text{Mg} + \text{Fe}^{2+})$] values varying from 62.3 up to 80.3, thus resembling spinels occurring in abyssal peridotites (Figure 5). They are also rather enriched in NiO contents (0.24–0.68 wt. %) and show an Mg#–Cr# linear trend (Figure 5). Low TiO₂ values in these spinels are explained by the coexistence of ilmenite, as Ti preferentially enters the crystal lattice of the last. Secondary Cr-spinels in the lherzolite, which are associated to serpentinisation, along cleavage of orthopyroxenes, show lower Mg# (51.2–60.0) and higher Cr# values (31.3–41.8) than the Al-spinels. These Cr-spinels are not shown in Figure 5 and are not further considered for the igneous petrogenetic processes discussed below.

The harzburgite includes two different generations of spinel-group minerals. The older one comprises Cr-spinel whereas the younger includes magnesiochromite (Cr# > 60 and Mg > Fe²⁺) and chromite (Cr# > 60 and Mg < Fe²⁺). The magnesiochromite and chromite are considered as one group, therefore they will collectively be mentioned as chromite hereafter. Unaltered Cr-spinels show an inter-grain chemical variation with Cr# ranging from 30.8 to 58.5 and Mg# from 47.1 to 70.4 (Figure 5). The chromite crystals plot into two distinctive clusters on their Mg# vs. Cr# diagram: (i) a Cr#-poorer and Mg#-richer group (Cr# = 63.7–65.6, Mg# = 58.1–63.4), which are texturally associated to the Cr-spinels and (ii) a Cr#-richer and Mg#-poorer one (Cr# = 68.6–74.9, Mg# = 40.5–54.2), which are the aforementioned individual euhedral crystals. The last group of euhedral crystals shows a chemical core-to-rim zonation with decreasing Al₂O₃, MgO and Cr₂O₃ and increasing FeO. The Cr-spinels

straddle the abyssal- and arc-derived SSZ peridotite fields showing much resemblance with spinels from forearc peridotites whereas the chromites plot entirely in the field of SSZ-related peridotites with the Cr-rich and Mg-poorer chromites showing considerable similarities with spinels from boninitic melts (Figure 5). Ferritchromit and magnetite have formed along fractures and rims of Cr-spinels and are enriched in Cr, Mn and rarer Zn.

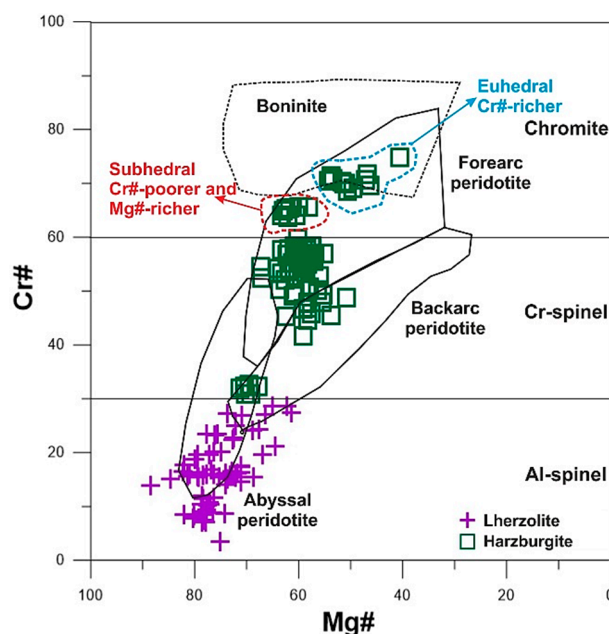


Figure 5. Compositional variations of spinel-group minerals from Edessa peridotites in a Cr# vs. Mg# diagram. Compositional fields for spinel-group minerals in boninite [24,41], forearc peridotite, backarc peridotite, and abyssal peridotite [42] are shown for comparison.

5.2. Pyroxenes

Representative clinopyroxene microanalyses from the investigated ultramafic rocks are listed in Table 2. The lherzolite includes mainly diopside with Mg# ranging from 89.2 up to 93.1. The porphyroclasts display generally higher (with overlaps) Al_2O_3 (3.45–6.60 wt. %) and TiO_2 (0.29–1.14 wt. %) contents than the neoblasts (Al_2O_3 : 1.46–4.12 wt. %, TiO_2 : 0.15–0.95 wt. %). Their CaO abundance ranges from 17.96 to 23.51 wt. %. Cr_2O_3 concentration varies from 0.41 to 1.12 wt. %, whereas Na_2O values are in high abundances (0.78–1.09 wt. %) only in porphyroclasts. The harzburgite contains porphyroclastic diopside with higher Mg# (93.0–94.5), Cr_2O_3 (0.57–1.39 wt. %) and lower Al_2O_3 contents (2.38–4.58 wt. %) than those in the lherzolite. On an Al_2O_3 vs. Mg# and a Cr_2O_3 vs. Mg# diagrams the majority of the analysed porphyroclastic clinopyroxenes from lherzolite resemble those occurring in abyssal peridotites whereas the neoblastic ones are poorer in Cr (with overlaps) and Al (Figure 6a,b). The harzburgitic diopsides show a more refractory nature and on a Cr_2O_3 vs. Mg# diagram they resemble clinopyroxenes originated in forearc peridotites (Figure 6b).

No fresh and sizeable relics of orthopyroxene have been detected in the harzburgite, to obtain reliable analyses. Representative orthopyroxene analyses from the lherzolite are listed in Table 3. They include enstatite with Mg# values ranging between 89.2 and 90.2, as well as moderate Al_2O_3 (2.10–5.07 wt. %) and CaO (0.29–1.10 wt. %), and relatively low TiO_2 (0.16–0.52 wt. %), MnO (0.27–0.33 wt. %) and Cr_2O_3 (0.11–0.57 wt. %) contents. On an Al_2O_3 vs. Mg# diagram the majority of the analysed orthopyroxene compositions plot within the abyssal peridotite field (Figure 6c), however their Cr_2O_3 -Mg# relationships are inconclusive (Figure 6d).

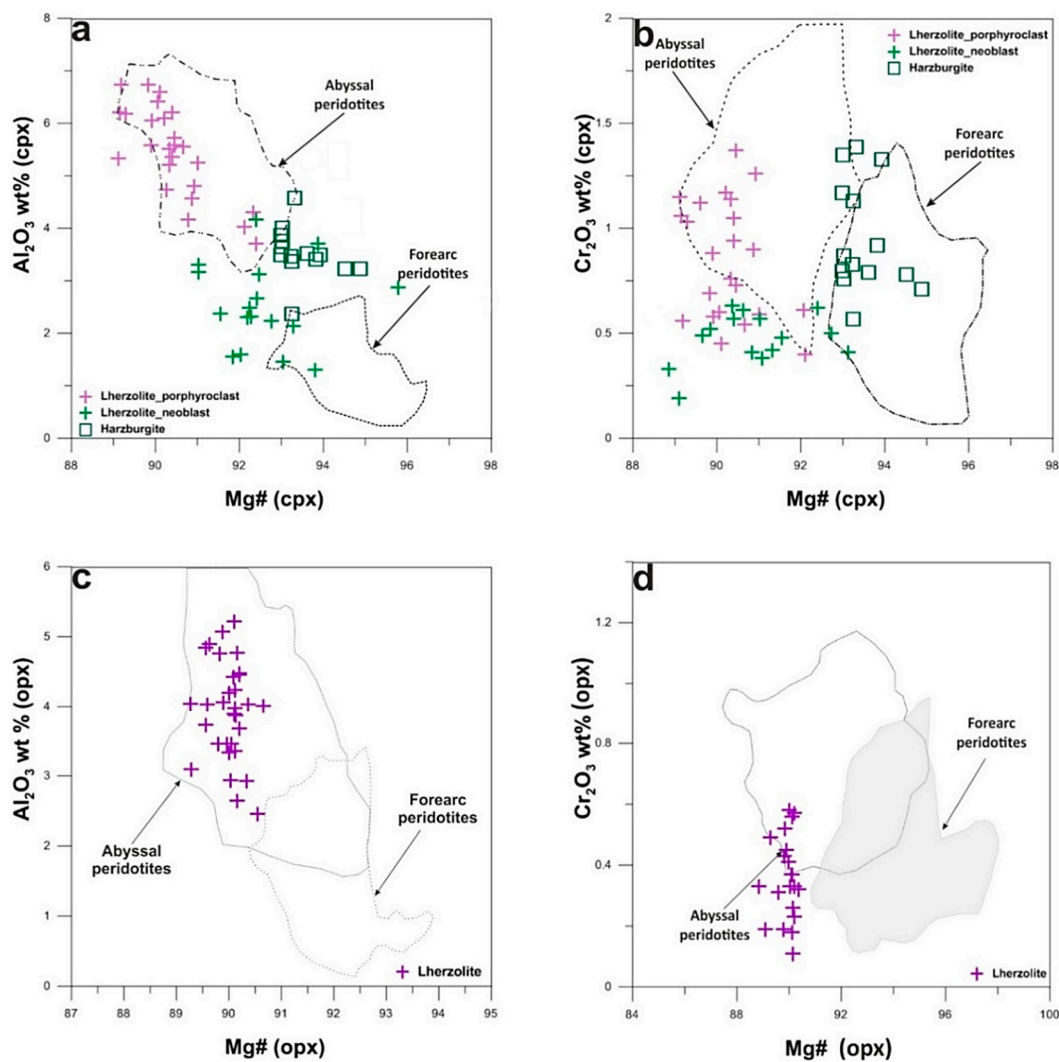


Figure 6. Compositional variations of clinopyroxene and orthopyroxene in peridotites from the Edessa ophiolite. (a) Al₂O₃ vs. Mg# for cpx; (b) Cr₂O₃ vs. Mg# for cpx; (c) Al₂O₃ vs. Mg# for opx; (d) Cr₂O₃ vs. Mg# for opx. Fields of forearc and abyssal peridotites are from Lian et al. [43]. Few pyroxene analyses with Al and/or Cr contents below detection limits are not plotted.

5.3. Olivine

Representative olivine analyses from the lherzolite are listed in Table 4. Forsterite (Fo) contents range from 88.9 to 90.4, which are similar to Fo values of olivines from typical supra-subduction zone SSZ peridotites (Fo = 87–94 according to Pirard et al. [44]). The analysed olivines, both porphyroclasts and neoblasts (Table 4), show a rather similar composition having very similar FeO (8.87–10.25 wt. %) and MgO (44.54–48.62 wt. %) contents. NiO contents ranging from 0.29 to 0.85 wt. %, are generally within the range of NiO concentrations for mantle olivines (0.25–0.51 wt. % according to De Hoog et al. [45]), with few exceptions, which show the higher NiO values. Few analyses of olivine neoblasts yielded NiO below detection limit. The NiO contents of olivine shows no correlation with the respective Fo values and a large number of several analyses are plotted in the field of abyssal peridotites (Figure 7). Again in the harzburgite we were unable to acquire reliable olivine analyses due to the lack of sizeable unaltered crystals.

Table 1. Representative electron microanalyses of spinel-group minerals from peridotites of the Edessa ophiolitic complex (-: below detection limit; *: degrees F of partial melting are not calculated for altered and chemically modified spinels).

Rock-Type	Lherzolite												Harzburgite					
Sample	ED.88						ED.89						BE.117					
Anal. NO.	14	16	28	38	54	79	92	28	30	34	36	66	90	1	3	4	5	6
wt. %	Al-sp	Al-sp	Al-sp	Al-sp	Al-sp	Cr-sp	Cr-sp	Al-sp	Al-sp	Al-sp	Al-sp	Al-sp	Al-sp	Cr-sp	Cr-sp	Cr-sp	Cr-sp	Cr-sp
TiO ₂	-	0.15	-	-	-	-	-	-	-	-	-	-	-	-	-	-	-	-
Al ₂ O ₃	59.03	50.70	42.31	56.25	56.29	31.78	40.39	52.39	44.74	56.71	54.82	58.79	57.81	41.17	39.65	40.93	39.88	41.47
FeO	12.15	14.17	17.57	12.48	12.68	22.58	19.35	15.15	16.05	13.48	13.48	11.35	13.46	13.70	14.54	13.95	13.86	14.51
MnO	-	0.14	-	-	-	-	-	-	-	-	-	-	-	-	-	0.20	0.34	-
MgO	20.01	18.74	14.86	19.36	20.18	11.50	14.34	18.60	16.22	19.87	19.15	20.55	20.34	16.64	16.42	16.77	15.61	16.53
Cr ₂ O ₃	7.11	16.15	25.30	8.58	10.87	34.01	27.41	14.51	21.47	9.64	10.72	7.44	10.34	27.44	28.55	27.17	28.24	27.59
NiO	0.44	0.27	-	0.59	0.24	-	-	-	-	0.52	0.38	0.53	-	0.25	0.18	0.20	0.34	0.44
Sum	98.74	100.2	100.04	97.26	100.26	99.87	101.49	100.65	98.48	100.22	98.55	98.66	101.95	99.20	99.34	99.26	98.27	100.54
Formula units based on 3 cations																		
Al	1.806	1.590	1.402	1.762	1.718	1.119	1.337	1.630	1.474	1.732	1.712	1.796	1.734	1.364	1.321	1.355	1.346	1.360
Ti	-	0.003	-	-	-	-	-	-	-	-	-	-	-	-	-	0.001	-	-
Cr	0.146	0.340	0.562	0.180	0.223	0.804	0.609	0.303	0.475	0.198	0.225	0.152	0.208	0.610	0.638	0.604	0.639	0.607
Fe ³⁺	0.048	0.064	0.036	0.057	0.059	0.077	0.055	0.067	0.051	0.071	0.063	0.051	0.058	0.025	0.040	0.038	0.014	0.033
Mg	0.775	0.743	0.623	0.767	0.779	0.512	0.600	0.732	0.676	0.768	0.756	0.794	0.772	0.698	0.692	0.702	0.666	0.686
Ni	0.009	0.006	-	0.013	0.005	-	-	-	-	0.011	0.008	0.011	-	0.006	0.004	0.005	0.008	0.010
Fe ²⁺	0.216	0.251	0.377	0.220	0.216	0.488	0.400	0.268	0.324	0.222	0.235	0.195	0.228	0.297	0.304	0.290	0.317	0.305
Mn	-	0.003	-	-	-	-	-	-	-	-	-	-	-	-	-	0.005	0.008	-
Cr#	7.5	17.6	28.6	9.3	11.5	41.8	31.3	15.7	24.4	10.2	11.6	7.8	10.7	30.9	32.6	30.8	32.2	30.9
Mg#	78.2	74.7	62.3	77.7	78.3	51.2	60.0	73.2	67.6	77.6	76.3	80.3	77.2	70.2	69.5	70.4	67.7	69.2
F	1	7	12	1	2	*	*	5	10	1	2	1	2	12	13	12	13	12

Table 1. Cont.

Rock-Type		Harzburgite															
Sample		ED.28.2						ED.33						ED.115			
Anal. No.	6	51	101	124	145	12	58	60	1	3	16	20	1	3	4	16	17
wt. %	Cr-sp	Cr-sp	Cr-sp	Cr-sp	Cr-sp	Fe-chr	Fe-chr	Fe-chr	Cr-sp	Cr-sp	Cr-sp	Fe-chr	Chr	Chr	Chr	Chr	Chr
Al ₂ O ₃	31.24	33.67	27.56	24.35	25.90	8.56	3.36	2.30	23.37	23.59	24.62	1.68	15.88	14.83	16.30	15.95	15.33
FeO	19.05	18.56	19.46	18.51	17.95	43.54	59.64	58.33	15.22	15.45	16.42	38.12	18.73	18.43	19.31	19.94	19.57
MnO	-	-	-	-	-	9.51	5.35	6.39	-	-	-	12.12	-	-	-	-	-
MgO	13.32	13.76	13.75	14.18	13.09	1.71	1.68	1.65	14.09	14.03	13.83	2.15	10.79	11.19	10.53	9.63	10.79
Cr ₂ O ₃	37.40	35.91	40.51	42.89	44.04	36.24	29.42	31.26	49.19	47.28	45.79	41.60	54.99	55.12	53.19	54.68	54.30
NiO	-	-	-	-	-	-	-	-	-	-	-	-	-	-	-	-	-
ZnO	-	-	-	-	-	-	-	-	-	-	-	3.02	-	-	-	-	-
Sum	101.01	101.90	101.28	99.93	100.98	99.56	99.45	99.93	101.87	100.35	100.66	98.69	100.39	99.57	99.33	100.20	99.99
Formula units based on 3 cations																	
Al	1.081	1.143	0.962	0.868	0.917	0.353	0.141	0.097	0.825	0.842	0.874	0.072	0.598	0.563	0.619	0.606	0.580
Cr	0.868	0.818	0.949	1.025	1.046	1.002	0.829	0.882	1.165	1.133	1.091	1.197	1.388	1.403	1.355	1.394	1.378
Fe ³⁺	0.051	0.038	0.089	0.107	0.037	0.645	1.029	1.021	0.010	0.025	0.035	0.731	0.014	0.034	0.026	-	0.042
Mg	0.583	0.591	0.607	0.639	0.586	0.089	0.089	0.088	0.629	0.634	0.621	0.117	0.514	0.537	0.506	0.463	0.516
Ni	-	-	-	-	-	-	-	-	-	-	-	-	-	-	-	-	-
Fe ²⁺	0.417	0.409	0.393	0.361	0.414	0.629	0.749	0.719	0.371	0.366	0.379	0.429	0.486	0.463	0.494	0.537	0.484
Mn	-	-	-	-	-	0.282	0.162	0.193	-	-	-	0.374	-	-	-	-	-
Zn	-	-	-	-	-	-	-	-	-	-	-	0.081	-	-	-	-	-
Cr#	44.5	41.7	49.6	54.2	53.3	74.0	85.5	90.1	58.5	57.4	55.5	94.3	69.9	71.4	68.6	69.7	70.4
Mg#	58.3	59.1	60.7	63.9	58.6	12.4	10.7	10.9	62.9	63.4	62.1	21.4	51.4	53.7	50.6	46.3	51.6
F	16	15	17	18	18	*	*	*	19	18	18	*	*	*	*	*	*

Table 2. Representative electron microanalyses of clinopyroxenes from peridotites of the Edessa ophiolitic complex (-: below detection limit).

Rock-Type	Lherzolite						Harzburgite							
Sample	ED.88						ED.89			BE.117				
Anal. No	75	76	107	83	95	102	52	53	60	18	19	21	39	43
wt. %	Porph.	Porph.	Porph.	Porph.	Porph.	Porph.	Neobl.	Neobl.	Neobl.	Porph.	Porph.	Porph.	Porph.	Porph.
SiO ₂	54.13	53.59	52.78	54.71	53.38	52.04	54.66	53.59	55.44	52.18	52.76	52.56	55.44	52.81
TiO ₂	0.71	0.64	1.14	0.67	0.49	0.29	0.15	0.95	0.25	-	-	-	-	-
Al ₂ O ₃	6.05	6.60	5.25	1.74	4.71	6.21	2.30	2.60	1.46	4.58	3.47	3.65	2.38	3.23
FeO	3.06	2.70	2.61	2.53	2.69	2.92	2.28	2.33	2.21	2.06	2.07	2.23	2.12	1.66
MgO	15.30	13.80	14.81	16.49	15.01	13.46	16.29	15.88	16.81	16.16	15.99	16.62	16.42	16.07
CaO	21.14	21.42	23.51	23.10	22.03	20.61	23.36	22.65	23.04	22.96	24.34	23.14	23.17	23.47
Na ₂ O	0.81	0.93	0.82	-	0.78	0.97	-	-	-	-	-	-	-	-
Cr ₂ O ₃	0.58	0.45	0.59	0.61	0.93	1.06	0.50	0.62	0.41	1.39	0.83	1.35	0.57	0.78
Sum	101.78	100.13	101.51	99.85	100.02	97.56	99.54	98.62	99.62	99.33	99.46	99.55	100.10	98.02
Formula units based on 6 oxygens														
Si	1.916	1.925	1.891	1.981	1.930	1.924	1.983	1.963	2.000	1.903	1.927	1.916	1.994	1.947
Al ^{iv}	0.084	0.075	0.109	0.019	0.070	0.076	0.017	0.037	-	0.097	0.073	0.084	0.006	0.053
Al ^{vi}	0.168	0.205	0.112	0.056	0.131	0.195	0.081	0.075	0.062	0.100	0.076	0.073	0.095	0.087
Fe ³⁺	-	-	-	-	-	-	-	-	-	-	-	-	-	-
Ti	0.019	0.017	0.031	0.018	0.013	0.008	0.004	0.026	0.007	-	-	-	-	-
Cr	0.016	0.013	0.017	0.017	0.027	0.031	0.014	0.018	0.012	0.040	0.024	0.039	0.016	0.023
Mg	0.807	0.739	0.791	0.890	0.809	0.742	0.881	0.867	0.906	0.879	0.871	0.903	0.880	0.883
Fe ²⁺	0.091	0.081	0.078	0.077	0.081	0.090	0.069	0.071	0.067	0.063	0.063	0.068	0.064	0.051
Ca	0.802	0.824	0.902	0.896	0.854	0.816	0.908	0.889	0.893	0.897	0.952	0.904	0.893	0.927
Na	0.056	0.065	0.057	-	0.055	0.070	-	-	-	-	-	-	-	-
En	47.5	44.9	44.7	47.8	46.4	45.0	47.4	47.5	48.6	47.8	46.2	48.2	47.9	47.4
Fs	5.3	4.9	4.4	4.1	4.7	5.5	3.7	3.9	3.6	3.4	3.4	3.6	3.5	2.7
Wo	47.2	50.1	50.9	48.1	48.9	49.5	48.9	48.6	47.9	48.8	50.5	48.2	48.6	49.8
Mg#	89.9	90.1	91.0	92.1	90.9	89.2	92.7	92.4	93.1	93.3	93.2	93.0	93.2	94.5

Table 3. Representative electron microanalyses of porphyroclastic orthopyroxenes from lherzolite of the Edessa ophiolitic complex (-: below detection limit).

Rock-Type		Lherzolite											
Sample		ED.88						ED.89					
Anal. No	16	17	19	101	102	104	111	14	24	46	68	69	70
wt. %	Porph.	Porph.	Porph.	Porph.	Porph.	Porph.	Porph.	Porph.	Porph.	Porph.	Porph.	Porph.	Porph.
SiO ₂	57.91	57.57	58.34	56.62	55.45	57.60	56.35	56.27	57.15	56.41	57.17	56.35	56.06
TiO ₂	-	0.16	0.23	-	0.52	-	-	-	-	0.29	-	-	-
Al ₂ O ₃	4.48	4.04	3.09	4.84	4.03	4.01	4.63	5.07	4.46	2.94	3.35	3.86	4.24
FeO	6.18	6.55	6.63	6.58	5.95	5.98	6.06	6.48	6.32	6.35	6.36	6.46	6.19
MnO	-	0.30	0.33	0.27	-	-	-	-	-	-	-	-	-
MgO	31.93	31.97	32.55	31.67	31.29	32.57	31.15	32.28	32.65	32.18	32.54	33.11	31.66
CaO	0.53	0.45	-	0.52	0.27	0.43	0.72	1.10	0.45	0.42	0.60	0.29	0.32
Na ₂ O	-	-	-	-	-	-	-	-	-	-	-	-	-
Cr ₂ O ₃	0.33	-	0.49	-	0.32	-	0.42	-	0.57	0.33	0.56	0.11	0.37
NiO	-	-	-	-	-	-	-	-	-	-	-	-	-
Sum	101.46	101.04	101.66	100.50	97.83	100.59	99.33	101.20	101.60	98.92	100.58	100.18	98.84
Formula units based on 6 oxygens													
Si	1.957	1.958	1.973	1.938	1.945	1.960	1.947	1.916	1.934	1.961	1.956	1.935	1.947
Al ^{iv}	0.043	0.042	0.027	0.062	0.055	0.040	0.053	0.084	0.066	0.039	0.044	0.065	0.053
Al ^{vi}	0.136	0.120	0.096	0.133	0.111	0.121	0.135	0.119	0.112	0.082	0.091	0.091	0.120
Fe ³⁺	-	-	-	-	-	-	-	-	-	-	-	-	-
Ti	-	0.004	0.006	-	0.014	-	-	-	-	0.008	-	-	-
Cr	0.009	-	0.013	-	0.009	-	0.011	-	0.015	0.009	0.015	0.003	0.010
Ni	-	-	-	-	-	-	-	-	-	-	-	-	-
Mg	1.609	1.621	1.641	1.616	1.636	1.652	1.604	1.638	1.647	1.668	1.659	1.695	1.639
Fe ²⁺	0.175	0.186	0.188	0.188	0.174	0.170	0.175	0.185	0.179	0.185	0.182	0.186	0.180
Mn	-	0.009	0.009	0.008	-	-	-	-	-	-	-	-	-
Ca	0.019	0.016	-	0.019	0.010	0.016	0.027	0.040	0.016	0.016	0.022	0.011	0.012
Na	-	-	-	-	-	-	-	-	-	-	-	-	-
En	89.3	88.5	89.3	88.3	89.9	89.9	88.8	87.9	89.4	89.3	89.1	89.6	89.5
Fs	9.7	10.6	10.7	10.7	9.6	9.3	9.7	9.9	9.7	9.9	9.8	9.8	9.8
Wo	1.1	0.9	0.00	1.0	0.6	0.9	1.5	2.2	0.9	0.8	1.2	0.6	0.6
Mg#	90.2	89.3	89.3	89.2	90.4	90.7	90.2	89.9	90.2	90.0	90.1	90.1	90.1

Table 4. Representative electron microanalyses of olivines from lherzolite of the Edessa ophiolitic complex (-: below detection limit).

Sample	ED.88							ED.89						
Anal. No	6	65	68	32	34	98	109	5	6	7	62	63	64	65
wt. %	Porph.	Porph.	Porph.	Neobl.	Neobl.	Neobl.	Neobl.	Porph.	Porph.	Porph.	Neobl.	Neobl.	Neobl.	Neobl.
SiO ₂	43.23	42.10	42.29	41.82	43.16	43.40	42.79	42.57	41.66	42.03	41.38	41.32	45.90	42.04
FeO	9.74	9.14	9.78	9.48	9.61	10.13	10.25	8.86	9.26	10.24	9.60	9.48	8.87	9.24
MnO	-	-	-	-	-	-	-	-	-	-	-	-	0.28	-
MgO	47.09	46.94	45.53	47.01	48.18	47.20	45.98	46.62	48.62	46.27	46.55	47.76	44.54	46.63
NiO	0.37	0.51	0.85	0.29	-	-	-	0.76	0.41	0.38	0.61	0.48	-	0.48
Sum	100.43	98.69	98.45	98.60	100.95	100.73	99.02	98.81	99.95	99.31	98.14	99.04	99.59	98.39
Formula units based on 4 oxygens														
Si	1.047	1.038	1.049	1.033	1.039	1.048	1.052	1.047	1.017	1.034	1.030	1.019	1.107	1.040
Mg	1.701	1.725	1.683	1.732	1.729	1.699	1.685	1.709	1.769	1.697	1.728	1.756	1.601	1.720
Fe ²⁺	0.197	0.188	0.203	0.196	0.193	0.205	0.211	0.182	0.189	0.211	0.200	0.196	0.179	0.191
Mn	-	-	-	-	-	-	-	-	-	-	-	-	0.006	-
Ni	0.007	0.010	0.017	0.006	-	-	-	0.015	0.008	0.008	0.012	0.010	-	0.010
Total	2.953	2.962	2.951	2.967	2.961	2.952	2.948	2.953	2.983	2.960	2.970	2.981	2.893	2.960
Fo	89.6	90.1	89.2	89.8	89.9	89.2	88.9	90.4	90.4	89.0	89.6	90.0	90.0	90.0
Fa	10.4	9.9	10.8	10.2	10.1	10.8	11.1	9.6	9.6	11.0	10.4	10.0	10.0	10.0

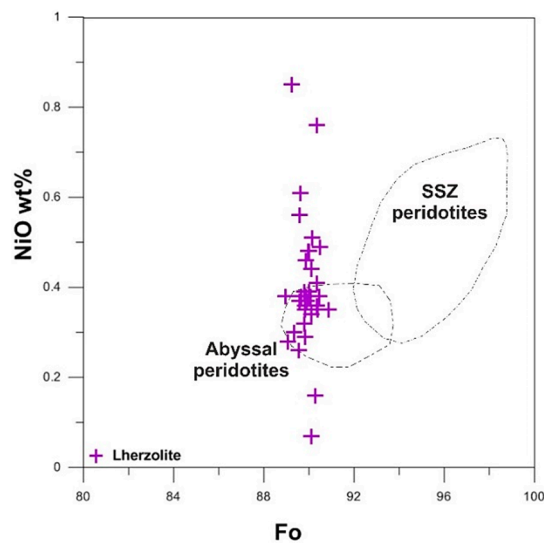


Figure 7. Compositional variations of olivines from the Edessa lherzolite in a Fo vs. NiO diagram. Abyssal and supra-subduction zone (SSZ) fields from Sobolev et al. [46] and Ishii et al. [47], respectively.

6. Geothermobarometry

Equilibration temperatures and pressure for the studied lherzolite were determined using the two-pyroxenes (clinopyroxene-orthopyroxene) geothermobarometer of Brey and Köhler [48] (Supplementary Table S1). Care was taken to select orthopyroxene porphyroclasts free of clinopyroxene exsolution lamellae. We selected co-existing mineral phases for the estimation of temperature and pressure, which have a well-defined common boundary with no evidence of alteration and similar Mg#, which indicate that they have attained equilibrium. Application of the two-pyroxene geothermobarometer yielded calculated temperatures varying between 942 and 1070 °C, assuming a pressure range of 0.9–1.4 GPa.

7. Discussion

7.1. Alteration Features of Spinel-Group Minerals

Spinel-group minerals are generally more resistant to alteration and/or metamorphism as compared to olivine and pyroxene [49–51]. Magnetite and Cr-bearing magnetite, are common alteration products of the spinel-group minerals in the two types of peridotites, whereas ferritchromit was observed only after Cr-spinel in harzburgite. Their formation is caused by a post-solidus state decomposition of the spinels in which Mg, Al and Cr diffuse out, hence Fe and other ions, such as Mn and Ni are enriched [52]. The narrow alteration zones of ferritchromit and magnetites imply a limited diffusion of these ions.

Ferritchromit rims in Cr-spinel grains generally contain elevated concentrations of Mn, Zn and Co [53,54]. The analysed harzburgitic Cr-spinel cores have lower contents of Mn and Zn compared to ferritchromit rims. In the absence of primary ilmenite in harzburgite, Cr-spinel is likely to be the favourable receptor for Mn. This may account for the observed high Mn-contents at the ferritchromit zone of harzburgite. Notable Mn-enrichments in the ferritchromit zones of harzburgitic Cr-spinel involve interaction of fluids that were likely rich in Mn [50,54,55]. Magnetite grows during serpentinisation from the excess Fe of the pre-existing olivine. Magnetite that rims spinels is a typical alteration product of spinels due to Cr and Al removal.

The occurrence of garnet at the rims and within micro-veins of Al-spinels in the lherzolite requires the existence of an influx characterised by substantial Ca-enrichment and Si-depletion. This has been documented within metasomatic lithologies known as rodingites [56–58] and indicates an initial stage of rodingitisation in associated gabbroic dykes.

7.2. Partial Melting of Mantle Peridotites

Partial melting of a mantle is controlled by various factors, such as pressure, temperature and water content, which can be used as diagnostic indicators of tectonic setting [59]. Partial melting beneath a mid-ocean ridge occurs at dry conditions, whereas a mantle wedge normally experiences hydrous melting due to the dehydration of the subducted slab. Thus, forearc mantle peridotites undergo higher degrees of partial melting relative to the oceanic mantle beneath a mid-ocean ridge [16,60]. Important information for mantle melting can be preserved by the modal mineralogy, mineral chemistry and whole-rock chemical composition. Clinopyroxene is generally considered to be the most rapidly consumed mineral specifically during the initial stages of partial melting [16,61]. It is known that Al contents of pyroxene and spinel are sensitive to the partial melting of mantle peridotites and they systematically decrease as the peridotites become more depleted [62,63]. Furthermore, forsterite contents of olivine and Cr# of spinel in peridotites are useful indicators of the degree of melting [41,42,64].

The variably depleted nature of the Edessa peridotites as evidenced by their mineralogical composition indicates that they are mantle residues after different degrees of melting. Variable amounts of remnant clinopyroxene occur in lherzolite, which gradually pass into harzburgites. The harzburgite has low clinopyroxene abundances (<5 vol. %) resembling mantle peridotites formed by high degrees of partial melting. On the contrary, the lherzolite has higher porphyroclastic clinopyroxene contents (5–15 vol. %) implying variable but small to moderate degrees of melt extraction [65,66]. Lobate boundaries of Al-spinel grains in the lherzolite, along with their linear Mg#–Cr# evolution, as well as their resemblance to abyssal peridotite spinels support the hypothesis of a partial melting episode during their genesis. The refractory nature of olivine (with Fo = 88.8–90.4 and high NiO) and orthopyroxenes (with Mg# = 89.2–90.2) in the lherzolite, are compatible with a partial melting episode. Moreover, the harzburgitic clinopyroxenes are more refractory (richer in Mg# and poorer in Al) than those in the lherzolite, hence suggesting that progressively increasing degrees of partial melting are responsible for the evolution of harzburgite (Figure 6a). The relatively low to moderate Al₂O₃ abundance in both orthopyroxene and clinopyroxene porphyroclasts of the lherzolites (Figure 6a,b), further advocate to the hypothesis that they have undergone considerable degrees of partial melting, thus representing upper mantle residues [67–69]. These clinopyroxene porphyroclasts in the lherzolite are similar to residual clinopyroxene in MOR-type peridotites, which underwent dry partial melting [70].

Moreover, it has been suggested that spinels in mantle peridotites become increasingly Cr-rich along with melting and thus Cr# in residual spinels is a sensitive indicator for the extent of melting of their host peridotites [41,42,71]. The Al-spinels from lherzolite show a broad range and a linear evolution of Cr# from 7.5 to 28.6, and Mg# from 62.3 to 80.3, strongly resembling spinels from peridotites forming in a MOR environment after low to moderate degrees of partial melting. The Cr-spinels in the harzburgite are thought to have a residual origin, as it is implied by their textural characteristics. They show higher Cr# than the Al-spinels, ranging from 30.9 to 58.5, and generally lower Mg# from 58.3 to 70.4, which are typical for spinel-group minerals from MOR-peridotites after high degrees of partial melting of an oceanic upper mantle source [64,72].

For the estimation of the degree of partial melting (F) for the lherzolite and harzburgite the Cr# in the spinel equation [$F = 10 \times \ln(\text{Cr}\#) + 24$] proposed by Hellebrand et al. [71] was used for our calculations. Our calculations confirm that the lherzolite has experienced lower degrees of partial melting (<12%; see Table 1) whereas the harzburgite has undergone higher degrees of partial melting than the lherzolite ranging from 12% to 19% (Table 1).

The olivine spinel mantle array (OSMA) diagram (Figure 8) proposed by Arai [41,64] based on Fo of olivine and Cr# of coexisting spinel is extensively employed to characterise mantle-derived, spinel-bearing peridotites, especially mantle restites on the basis of melting trend for a fertile MORB mantle. The Fo–Cr# fractionation trend reflects the differentiation of magma including various processes such as crystallisation differentiation, magma mixing and assimilation. The spinel-olivine

pairs in the lherzolite plot at the lower end of the abyssal peridotite field and overlap with the field of passive margin peridotites, further indicating the relatively fertile nature of the lherzolite. This plot is also consistent with the calculated low degrees of partial melting (<12%) mentioned above for the lherzolite (Figure 8 and Table 1).

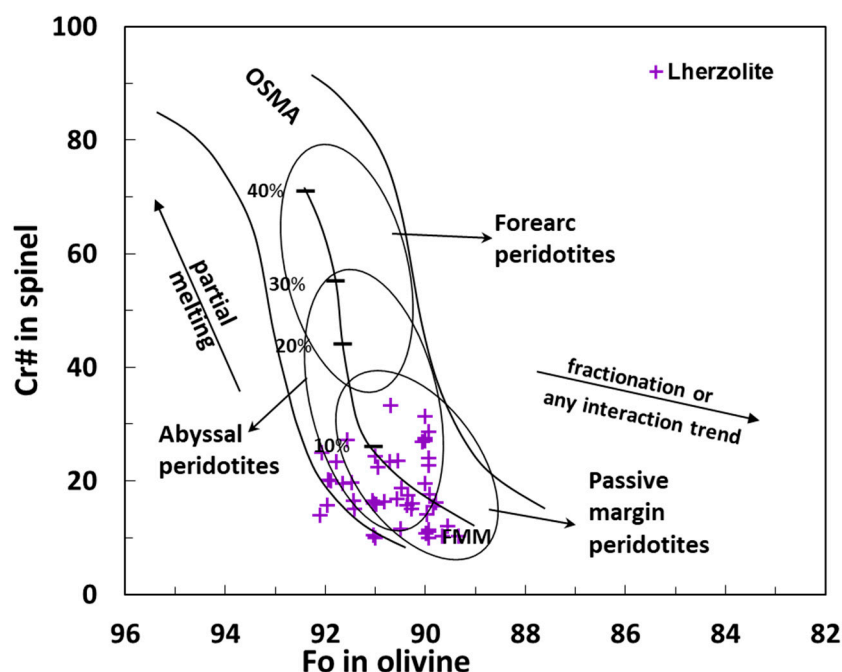


Figure 8. Plot of spinel Cr# against olivine Fo from the lherzolite of the Edessa ophiolite. Fields for abyssal peridotites [41,64], the forearc peridotites and passive continental margin peridotites [60] are also shown for comparison. The olivine-spinel mantle array (OSMA), partial melting trend and fractional lines are from Arai [41,64].

7.3. Evidence of Melt-Rock Reaction

The petrographic features and the mineralogical compositions in the Edessa peridotites documented in this study cannot be explained only by partial melting mechanisms. It is argued above that the Edessa lherzolite shows evidence for mantle melting textures. However, most orthopyroxene porphyroclasts exhibit characteristic textures including curved boundaries and partial replacement by olivine neoblasts (Figure 4c), which are interpreted as a result of a later-stage incongruent dissolution of pyroxenes, caused by reaction between a percolating melt and the minerals [66,73]. Fine-grained unstrained clinopyroxene and olivine occurring as interstitial crystals are thought to have been crystallised from these melts, which were trapped in the shallow mantle [74–76]. These microstructures in the Edessa lherzolite support the hypothesis that a Si-poor basaltic melt passed through the lherzolite during its ascent in the shallow mantle and has interacted with primary minerals, resulting in resorption of orthopyroxene and the precipitation of fine-grained clinopyroxene and olivine.

Moreover, the band-like olivine aggregates occurring in a few samples of lherzolite, likely represent the melt migrating channels within the mantle. These dunite veins in the lherzolite may reflect the interaction of rising mantle melts with lherzolite, which traveled adiabatically upwards dissolving pyroxenes, thus becoming saturated in olivine [77]. The observed dunite melt channels were formed upon olivine crystallisation and as soon as they were completely surrounded by olivine, melts effectively ceased to interact with their wallrocks, hence travelling upwards in a nearly closed-system.

Changes in the spinel-group minerals habits and composition may also reflect some variations in the peridotites [78]. Apart from melt extraction mentioned earlier, the Cr# of modified spinel-group minerals has been shown to be a sensitive indicator for melt-peridotite reaction during porous flow and melt-wallrock reactions in the vicinity of intruding magmatic veins [79–81]. Spinel formation

by reaction with a migrating silicate liquid records enrichment in Cr and a concomitant decrease in Al. Unlike the Al- and Cr-spinels, whose chemical affinities are explained in terms of partial melting, the chromites in the harzburgite, which record enrichment in Cr and a concomitant decrease in Al, are likely the result of (re)crystallisation during melt-rock interactions, as it is implied by their generally euhedral habit. The Cr#-richer and Mg#-poorer chromites (Figure 5) resemble spinels from arc peridotites. Therefore, it is suggested that a Si-rich melt with boninitic affinity percolated through the Edessa mantle sequence producing the Cr-rich compositions of the euhedral chromite, as it is commonly interpreted in studies of other similar environments [27,68,69]. Furthermore, the local modification of chromite (the Cr#-poorer and Mg#-richer cluster described in Figure 5) is compatible with the impregnation by such a Cr-rich melt. The percolating melt likely became locally saturated with chromite, as a result of the rock-melt reaction, hence increasing the Cr#'s of the pre-existing residual Cr-spinels. The elevated Cr# and the low-Ti contents in the chromites are compatible with their crystallisation from a low-Ti, boninitic melt [60].

7.4. Geotectonic Implications

Ophiolite complexes represent fragments of oceanic lithosphere emplaced on the continental crust, and their origins have been assigned to a variety of tectonic settings [6]. The modal and elemental composition of the mineral constituents of mantle peridotites are dependent on the geotectonic environment of their formation. Al–Mg and Cr–Mg relationships of the porphyroclastic pyroxenes, as well as Ni contents of olivine, support that lherzolites formed in a mid-oceanic spreading center by lower degrees of partial melting, whereas the more refractory nature of porphyroclastic clinopyroxenes in the harzburgites (Figure 6a,b) suggest an origin in a forearc setting by higher degrees of partial melting. Neoblastic clinopyroxenes in the lherzolite show lower Cr and Al contents than the porphyroclasts, which is interpreted as a result of their crystallisation presumably from a MORB-like melt, which impregnated the peridotite. Melts that evolve in a single environment are expected to be more differentiated leading normally to formation of olivine neoblasts, which are poorer in Fo than the porphyroclasts in a rock. However, MgO and FeO contents of olivine neoblasts in the lherzolite do not differ significantly from those of the porphyroclastic ones, thus showing similar Fo contents.

The Cr# in spinel-group minerals is a good indicator of the tectonomagmatic history of the host rock. The Al-spinel in the lherzolite and the Cr-spinel in the harzburgite display low Cr# (<60), typical of oceanic ophiolites (including back-arc basins [42]). It is argued above that the Al-spinels from the lherzolite are residues after low to moderate degrees of partial melting in a spreading environment. The origin of the residual Cr-spinels of the harzburgites (including the cpx-bearing ones) with Cr# clustering between 30.9 and 58.5 (Figure 5) require higher degrees of melting (up to 19%), which are consistent with an arc setting and hydrous conditions [82]. The existence of the subhedral to anhedral chromites (Cr#-poorer–Mg#-richer in Figure 5) indicate a chemical modification of Cr-spinels after interaction with a Cr-rich melt and is in line with this interpretation. Crystallisation of euhedral chromites (Cr#-richer–Mg#-poorer in Figure 5) indicates that apparently this melt became saturated in Cr. This fact strongly favours the involvement of a reactive, percolating boninitic melt, which can only be generated in a mantle wedge above a subduction zone.

Therefore, it is proposed that the lherzolites were generated in the Mesozoic Tethys ocean spreading environment and underwent a first stage of melting followed by interaction with a Si-poor (presumably MORB-like) melt. Most likely, these rocks were subsequently migrated in the forearc region above a subduction zone and were subjected to more extensive melt extraction under hydrous conditions. In this environment a melt with boninitic affinity reacted with the rocks overprinting the lherzolite and the harzburgite.

The coexistence of both MOR- and SSZ-type peridotites has also been reported in other ophiolite suites, such as Troodos [83] and SW Turkey [63,69]. These suites have a complex evolution involving both spreading and converging regimes similar to the Edessa peridotites. Previous studies from modern forearc settings have shown that those peridotites may have a variety of origins, ranging from

abyssal to SSZ regimes and have experienced hydrous melting in the mantle wedge [16,25,60,84–87]. These peridotites display textural, mineralogical and compositional characteristics for multi-phase melting, depletion and enrichment processes in their petrogenesis similar to those observed in the Edessa peridotites [69,88]. Abyssal peridotites might represent ocean lithosphere trapped above the subduction zone at initiation, or accretion to the upper plate during plate convergence at a later time [16]. Furthermore, abyssal peridotites can also be juxtaposed with SSZ peridotites during collision of a spreading center with a subduction zone [89].

8. Conclusions

The Edessa ophiolite is dominated by peridotites. Crustal suite rocks include minor gabbro and diorite, as well as diabase and basalt. The mantle section is composed mainly of harzburgite and minor lherzolite. The lherzolite is considered as the product of a first stage melting that occurred probably in a mid-ocean ridge environment. The Al- and Cr-poor nature of the neoblastic clinopyroxenes and the rather rich in Fo-rich nature of neoblastic olivines in the lherzolite strongly support the hypothesis for impregnation from an Mg-rich and Si-poor melt, likely of MORB origin. Subsequently, harzburgites were formed by more complicated processes including higher degrees (12–20%) of melting and additional modification by melt-rock interaction, in a supra-subduction zone (SSZ) environment. The lherzolite contains Al-spinels with moderate Cr# values, which indicate varying degrees of melting up to 12%. The Cr# values of the Cr-spinels and chromite from the harzburgite are higher than the lherzolite. The harzburgite is interpreted as the product of at least two stages of melting, including an early anhydrous event followed by a hydrous one. The lower Al₂O₃ and higher Mg# of the harzburgitic clinopyroxenes, as well as the more refractory olivine in the harzburgite relative to those in the lherzolite are consistent with this interpretation and an origin in a SSZ environment.

The co-existence of both MOR- and SSZ-type peridotites in the Edessa ophiolite supports the hypothesis that they have experienced a complicated evolution in a spreading oceanic basin to eventually the mantle wedge above a subduction zone. This scenario appears to be common for most of the Neo-Tethyan ophiolites as they are highly heterogeneous in their mantle compositions, melt evolution patterns and collisional histories.

Supplementary Materials: The following are available online at <http://www.mdpi.com/2075-163X/9/2/120/s1>, Table S1: Geothermobarometer.

Author Contributions: A.R. participated in the fieldwork, the interpretation of the results, coordinated the research and wrote the paper; P.P. participated in the fieldwork and performed the SEM work; B.T. participated in the fieldwork, in the interpretation of the results and wrote the paper; P.P.G. participated in the fieldwork and K.H. participated in the interpretation of the results.

Funding: This research received no external funding.

Acknowledgments: The authors are grateful to three anonymous referees who have substantially revised an earlier version of the manuscript. We thank Claudio Marchesi (guest editor) for his recommendations and editorial handling. We also thank Federica Zaccarini for her recommendations and suggestions. We kindly thank A.K. Seferlis of the Laboratory of Electron Microscopy and Microanalysis, University of Patras for his assistance with the microanalyses and SEM micrographs. We also thank M. Kalpogiannaki for her assistance with the construction of the geological map. A. Rogkala was financially supported by the Greek State Scholarship Foundation (IKY) during her Ph.D. study.

Conflicts of Interest: The authors declare no conflict of interest.

References

1. Dilek, Y.; Eddy, C.A. The Troodos (Cyprus) and Kizildag (S. Turkey) ophiolites as structural models for slow-spreading ridge segments. *J. Geol.* **1992**, *100*, 305–322. [[CrossRef](#)]
2. Pelletier, L.; Vils, F.; Kalt, A.; Gmeling, K. Li, B and Be contents of harzburgites from the Dramala Complex (Pindos Ophiolite, Greece): Evidence for a MOR-type mantle in a supra-subduction zone environment. *J. Petrol.* **2008**, *49*, 2043–2080. [[CrossRef](#)]

3. Dilek, Y.; Furnes, H. Ophiolite genesis and global tectonics: geochemical and tectonic fingerprinting of ancient oceanic lithosphere. *Geol. Soc. Am. Bull.* **2011**, *123*, 387–411. [[CrossRef](#)]
4. Ahmed, A.H. Highly depleted harzburgite-dunite-chromitite complexes from the Neoproterozoic ophiolite, south Eastern Desert, Egypt: a possible recycled upper mantle lithosphere. *Precambrian Res.* **2013**, *233*, 173–192. [[CrossRef](#)]
5. Dai, J.; Wang, C.; Polat, A.; Santosh, M.; Li, Y.; Ge, Y. Rapid forearc spreading between 130 and 120 Ma: evidence from geochronology and geochemistry of the Xigaze ophiolite, southern Tibet. *Lithos* **2013**, *172–173*, 1–16. [[CrossRef](#)]
6. Dilek, Y.; Furnes, H. Ophiolites and their origins. *Elements* **2014**, *10*, 93–100. [[CrossRef](#)]
7. Ribeiro, A.; Munhá, J.; Fonseca, P.E.; Araújo, A.; Pedro, J.C.; Mateus, A.; Tassinari, C.; Machado, C.; Jesus, A. Variscan ophiolite belts in the Ossa-Morena Zone (Southwest Iberia): Geological characterization and geodynamic significance. *Gondwana Res.* **2010**, *17*, 408–421. [[CrossRef](#)]
8. Pearce, J.A.; Robinson, P.T. The Troodos ophiolite complex probably formed in a subduction initiation, slab edge setting. *Gondwana Res.* **2010**, *18*, 60–81. [[CrossRef](#)]
9. Chetty, T.R.K.; Yellappa, T.; Nagesh, P.; Mohanty, D.P.; Venkatasivappa, V.; Santosh, M.; Tsunogae, T. Structural anatomy of a dismembered ophiolite suite from Gondwana: The Manamedu complex, Cauvery suture zone, southern India. *J. Asian Earth Sci.* **2011**, *42*, 176–190. [[CrossRef](#)]
10. Saccani, E.; Beccaluva, L.; Photiades, A.; Zeda, O. Petrogenesis and tectono-magmatic significance of basalts and mantle peridotites from the Albania-Greek ophiolites and sub-ophiolitic mélanges. New constraints for the Triassic-Jurassic evolution of the Neo-Tethys in the Dinaride sector. *Lithos* **2011**, *124*, 227–242. [[CrossRef](#)]
11. Allahyari, K.; Saccani, E.; Rahimzadeh, B.; Zeda, O. Mineral chemistry and petrology of highly magnesian ultramafic cumulates from the Sarve-Abad (Sawlava) ophiolites (Kurdistan, NW Iran): New evidence for boninitic magmatism in intra-oceanic fore-arc setting in the Neo-Tethys between Arabia and Iran. *J. Asian Earth Sci.* **2014**, *79*, 312–328. [[CrossRef](#)]
12. Magganas, A.; Koutsovitis, P. Composition, melting and evolution of the upper mantle beneath the Jurassic Pindos ocean inferred by ophiolitic ultramafic rocks in East Othris, Greece. *Int. J. Earth Sci.* **2015**, *104*, 1185–1207. [[CrossRef](#)]
13. Arai, S.; Kadoshima, K.; Moeishita, T. Widespread arc-related melting in the mantle section of the northern Oman ophiolite as inferred from detrital chromian spinels. *J. Geol. Soc. Lond.* **2006**, *163*, 869–879. [[CrossRef](#)]
14. Uysal, I.; Kaliwoda, M.; Karsli, O.; Tarkian, M.; Sadiklar, M.B.; Ottley, C.J. Compositional variations as a result of partial melting and melt-peridotites interaction in an upper mantle section from the Ortaca area, southwestern Turkey. *Canad. Mineral.* **2007**, *45*, 1791–1813. [[CrossRef](#)]
15. Kelemen, P.B.; Dick, H.J.B.; Quick, J.E. Formation of harzburgite by pervasive melt/rock reaction in the upper mantle. *Nature* **1992**, *358*, 635–641. [[CrossRef](#)]
16. Parkinson, I.J.; Pearce, J.A. Peridotites from the Izu-Bonin-Mariana forearc (ODP Leg 125): evidence for mantle melting and melt-mantle interaction in a supra-subduction zone setting. *J. Petrol.* **1998**, *39*, 1577–1618. [[CrossRef](#)]
17. Niu, Y. Bulk-rock major and trace element compositions of abyssal peridotites: implications for mantle melting, melt extraction and post-melting processes beneath mid-ocean ridges. *J. Petrol.* **2004**, *45*, 2423–2458. [[CrossRef](#)]
18. Dupuis, C.; Hébert, R.; Dubois-Côté, V.; Guilmette, C.; Wang, C.S.; Li, Y.L.; Li, Z.J. The Yarlung Zangbo Suture Zone ophiolite mélange (southern Tibet): new insights from geochemistry of ultramafic rocks. *J. Asian Earth Sci.* **2005**, *25*, 937–960. [[CrossRef](#)]
19. Singh, A.K.; Nayak, R.; Khogenkumar, S.; Subramanyam, K.S.V.; Thakur, S.S.; Singh, R.K.B.; Satyanarayanan, M. Genesis and tectonic implications of cumulate pyroxenites and tectonite peridotites from the Nagaland-Manipur ophiolites, Northeast India: constraints from mineralogical and geochemical characteristics. *Geol. J.* **2017**, *52*, 415–436. [[CrossRef](#)]
20. Deschamps, F.; Godard, M.; Guillot, S.; Hattori, K. Geochemistry of subduction zone serpentinites: A review. *Lithos* **2013**, *178*, 96–127. [[CrossRef](#)]
21. Petrounias, P.; Giannakopoulou, P.P.; Rogkala, A.; Stamatis, P.M.; Tsikouras, B.; Papoulis, D.; Lampropoulou, P.; Hatzipanagiotou, K. The influence of alteration of aggregates on the quality of the concrete: A case study from serpentinites and andesites from central Macedonia (North Greece). *Geosciences* **2018**, *8*, 115. [[CrossRef](#)]

22. Petrounias, P.; Giannakopoulou, P.P.; Rogkala, A.; Lampropoulou, P.; Koutsopoulou, E.; Papoulis, D.; Tsikouras, B.; Hatzipanagiotou, K. The Impact of Secondary Phyllosilicate Minerals on the Engineering Properties of Various Igneous Aggregates from Greece. *Minerals* **2018**, *8*, 329. [[CrossRef](#)]
23. Giannakopoulou, P.P.; Petrounias, P.; Rogkala, A.; Tsikouras, B.; Stamatis, P.M.; Pomonis, P.; Hatzipanagiotou, K. The influence of the mineralogical composition of ultramafic rocks on their engineering performance: A case study from the Veria-Naousa and Gerania ophiolite complexes (Greece). *Geosciences* **2018**, *8*, 251. [[CrossRef](#)]
24. Barnes, S.J.; Roeder, P.L. The range of spinel compositions in terrestrial mafic and ultramafic rocks. *J. Petrol.* **2001**, *42*, 2279–2302. [[CrossRef](#)]
25. Ghosh, B.; Morishita, T.; Bhatta, K. Significance of chromian spinels from the mantle sequence of the Andaman Ophiolite, India: Paleogeodynamic implications. *Lithos* **2013**, *164–167*, 86–96. [[CrossRef](#)]
26. Zhou, M.F.; Robinson, P.T.; Bai, W.J. Formation of podiform chromitites by melt/rock interaction in the upper mantle. *Miner. Depos.* **1994**, *29*, 98–101. [[CrossRef](#)]
27. Kariipi, S.; Tsikouras, B.; Hatzipanagiotou, K.; Grammatikopoulos, T.A. Petrogenetic significance of spinel-group minerals from the ultramafic rocks of the Iti and Kallidromo ophiolites (Central Greece). *Lithos* **2007**, *99*, 136–149. [[CrossRef](#)]
28. Oh, C.W.; Rajesh, V.J.; Seo, J.; Choi, S.G.; Lee, J.H. Spinel compositions and tectonic relevance of the Bibong ultramafic bodies in the Hongseong collision belt, South Korea. *Lithos* **2010**, *117*, 198–208. [[CrossRef](#)]
29. Pomonis, P.; Magganas, A. Petrogenetic Implications for Ophiolite Ultramafic Bodies from Lokris and Beotia (Central Greece) Based on chemistry of their Cr-spinels. *Geosciences* **2017**, *7*, 10. [[CrossRef](#)]
30. Guo, G.; Liu, X.; Yang, J.; Pan, J.; Fan, X.; Zhou, W.; Duan, G. Tectonic discrimination of chromian spinels, olivines and pyroxenes in the Northeastern Jiangxi Province ophiolite, South China. *Miner. Petrol.* **2017**, *111*, 325–336. [[CrossRef](#)]
31. Rogkala, A.; Petrounias, P.; Tsikouras, B.; Hatzipanagiotou, K. Petrogenetic significance of spinel from serpentinised peridotites from Veria-Naousa ophiolite. *Bull. Geol. Soc. Gr.* **2016**, *50*, 1999–2008.
32. Saccani, E.; Photiades, A.; Santato, A.; Zeda, O. New evidence for supra-subduction zone ophiolites in the Vardar zone of northern Greece: implications for the tectonomagmatic evolution of the Vardar oceanic basin. *Ophioliti* **2008**, *33*, 65–85.
33. Michailidis, K.M. Zoned chromites with high Mn-contents in the Fe-Ni-Cr-laterite ore deposits from the Edessa area in Northern Greece. *Miner. Depos.* **1990**, *25*, 190–197. [[CrossRef](#)]
34. Végely, P. Origine “vardarienne”, chevauchement vers l’Ouest et r etrocharriage vers l’Est des ophiolites de Mac edoine (Gr ece) au cours du Jurassique sup erieur-Eocr etac e. *CR Acad. Sci. Paris* **1976**, *280*, 1063–1066.
35. Decourt, J.; Aubouin, J.; Savoyat, E. Le sillon m eso-hell enique et la zone p elagienne. *Bull. Soc. G eol. Fr.* **1977**, *1*, 32–70.
36. Pe-Piper, G.; Piper, D.J.W. *The Igneous Rocks of Greece: The Anatomy of an Orogen*; Gebrueder Borntraeger: Berlin/Stuttgart, Germany, 2002.
37. Rogkala, A.; Petrounias, P.; Tsikouras, B.; Hatzipanagiotou, K. New occurrence of pyroxenites in the Veria-Naousa ophiolite (north Greece): Implications on their origin and petrogenetic evolution. *Geosciences* **2017**, *7*, 92. [[CrossRef](#)]
38. Mercier, J.L.; Vergely, P. *Geological Map of Greece, Edhessa Sheet, 1:50.000*; IGME: Athens, Greece, 1984.
39. Brunn, J.H. *Geological Map of Greece, Veroia Sheet, 1:50.000*; IGME: Athens, Greece, 1982.
40. Eleftheriadis, G.; Castorina, F.; Soldatos, T.; Masi, U. Geochemical and Sr-Nd isotopic evidence for the genesis of the Late Cainozoic Almopia volcanic rocks (Central Macedonia, Greece). *Miner. Petrol.* **2003**, *78*, 21–36. [[CrossRef](#)]
41. Arai, S. Characterization of spinel peridotites by olivine-spinel compositional relationships: review and interpretation. *Chem. Geol.* **1994**, *113*, 191–204. [[CrossRef](#)]
42. Dick, H.J.B.; Bullen, T. Chromian spinel as a petrogenetic indicator in abyssal peridotites and spatially associated lavas. *Contrib. Mineral. Petrol.* **1984**, *86*, 54–76. [[CrossRef](#)]
43. Lian, D.; Yang, J.; Robinson, P.T.; Liu, F.; Xiong, F.; Zhang, L.; Gao, J.; Wu, W. Tectonic evolution of the western Yarlung Zangbo Ophiolitic Belt, Tibet: implications from the petrology, mineralogy, and geochemistry of peridotites. *J. Geol.* **2016**, *124*, 353–376. [[CrossRef](#)]
44. Pirard, C.; Hermann, J.; O’Neil, H.S.C. Petrology and Geochemistry of the Crust-Mantle Boundary in a Nascent Arc, Massif du Sud Ophiolite, New Caledonia, SW Pacific. *J. Petrol.* **2013**, *54*, 1759–1792. [[CrossRef](#)]

45. De Hoog, J.C.M.; Gall, L.; Cornell, D. Trace element geochemistry of mantle olivine and applications to mantle petrogenesis and geothermobarometry. *Chem. Geol.* **2010**, *270*, 196–215. [[CrossRef](#)]
46. Sobolev, A.V.; Hofmann, A.W.; Sobolev, S.V.; Nikogosian, I.K. An olivine-free mantle source of Hawaiian shield basalts. *Nature* **2005**, *434*, 590–597. [[CrossRef](#)] [[PubMed](#)]
47. Ishii, T.; Robinson, P.T.; Maekawa, H.; Fiske, R. Petrological Studies of Peridotites from Diapiric Serpentinite Seamounts in the Izu-Mariana Fore-arc, Leg 125. In *Proceedings of the Ocean Drilling Program. Scientific Results 125*; 1992, pp. 445–485. Available online: http://www-odp.tamu.edu/publications/125_SR/VOLUME/CHAPTERS/sr125_27.pdf (accessed on 17 February 2019).
48. Brey, G.P.; Köhler, T. Geothermobarometry in four-phase lherzolites. II. New thermobarometers and practical assessment of existing thermobarometers. *J. Petrol.* **1990**, *31*, 1353–1378. [[CrossRef](#)]
49. Mellini, M.; Rumori, C.; Viti, C. Hydrothermally reset magmatic spinels in retrograde serpentinites: Formation of “ferritchromit” rims and chlorite aureoles. *Contrib. Mineral. Petrol.* **2005**, *149*, 266–275. [[CrossRef](#)]
50. Banerjee, R.; Ray, D.; Ishii, T. Mineral Chemistry and Alteration Characteristics of Spinel in Serpentinised Peridotites from the Northern Central Indian Ridge. *J. Geol. Soc. India* **2015**, *86*, 41–51. [[CrossRef](#)]
51. Barnes, S.J. Chromite in komatiites. II. Modification during greenschist to mid-amphibolite facies metamorphism. *J. Petrol.* **2000**, *41*, 387–409. [[CrossRef](#)]
52. Sabah, A.I. Chemistry of accessory chromian spinel in serpentinites from the Panjwen ophiolite rocks, Zagros thrust zone, northeastern Iraq. *J. Kirkuk University-Scientific Studies* **2009**, *4*, 1–21.
53. Economou-Eliopoulos, M. Apatite and Mn, Zn, Co-enriched chromite in Ni Laterites of northern Greece and their genetic significance. *J. Geochem. Explor.* **2003**, *80*, 41–54. [[CrossRef](#)]
54. Gahlan, H.A.; Arai, S. Genesis of peculiarly zoned Co, Zn and Mn-rich chromian spinel in serpentinite of Bou-Azzer ophiolite, Anti-Atlas, Morocco. *J. Miner. Petrol. Sci.* **2007**, *102*, 69–85. [[CrossRef](#)]
55. Barra, F.; Gervilla, F.; Hernández, E.; Reich, M.; Padrón-Navarta, J.A.; González-Jiménez, J.M. Alteration patterns of chromian spinels from La Cabana peridotite, south-central Chile. *Miner. Petrol.* **2014**, *108*, 819–836. [[CrossRef](#)]
56. Li, X.P.; Zhang, L.; Wei, C.; Ai, Y.; Chen, J. Petrology of rodingite derived from eclogite in western Tianshan, China. *J. Metamorph. Geol.* **2007**, *25*, 363–382. [[CrossRef](#)]
57. Tsikouras, B.; Karipi, S.; Rigopoulos, I.; Perraki, M.; Pomonis, P.; Hatzipanagiotou, K. Geochemical processes and petrogenetic evolution of rodingite dykes in the ophiolite complex of Othrys (Central Greece). *Lithos* **2009**, *113*, 540–554. [[CrossRef](#)]
58. Tsikouras, B.; Karipi, S.; Hatzipanagiotou, K. Evolution of rodingites along stratigraphic depth in the Iti and Kallidromon ophiolites (Central Greece). *Lithos* **2013**, *175–176*, 16–29. [[CrossRef](#)]
59. Choi, S.H.; Shervais, J.W.; Mukasa, S.B. Supra-subduction and abyssal mantle peridotites of the Coast Range ophiolite, California. *Contrib. Mineral. Petrol.* **2008**, *156*, 551–576. [[CrossRef](#)]
60. Pearce, J.A.; Barker, P.F.; Edwards, S.J.; Parkinson, I.J.; Leat, P.T. Geochemistry and tectonic significance of peridotites from the South Sandwich arc-basin system, south Atlantic. *Contrib. Mineral. Petrol.* **2000**, *139*, 36–53. [[CrossRef](#)]
61. Baker, M.B.; Stolper, E.M. Determining the composition of high-pressure mantle melts using diamond aggregates. *Geochim. Cosmochim. Acta* **1994**, *58*, 2811–2827. [[CrossRef](#)]
62. Dick, H.J.B.; Natland, J.H. Late stage melt evolution and transport in the shallow mantle beneath the East Pacific Rise. In *Proceedings-Ocean Drilling Program Scientific Results*; National Science Foundation: Alexandria, VA, USA, 1996; pp. 103–134.
63. Uysal, I.; Ersoy, E.Y.; Karsli, O.; Dilek, Y.; Burhan Sadiklar, M.; Ottley, C.J.; Tiepolo, M.; Meisel, T. Coexistence of abyssal and ultra-depleted SSZ type mantle peridotites in a neo-Tethyan ophiolite in SW Turkey: constraints from mineral composition, whole-rock geochemistry (major-rare-REE-PGE), and Re-Os isotope systematics. *Lithos* **2012**, *132–133*, 50–69. [[CrossRef](#)]
64. Arai, S. Compositional variation of olivine-chromian spinel in Mg-rich magma as guide to their residual spinel peridotites. *J. Geol. Soc. Lond.* **1994**, *163*, 869–879. [[CrossRef](#)]
65. Dokz, A.; Uysal, I.; Kaliwoda, M.; Karsli, O.; Ottley, C.J.; Kandemir, R. Early abyssal- and late SSZ-type vestiges of the Rheic oceanic mantle in the Variscanbasement of the Sakaryan Zone, NE Turkey: Implications for the sense of subduction and opening of the Paleotethys. *Lithos* **2011**, *127*, 176–191. [[CrossRef](#)]

66. Seyler, M.; Lorand, J.P.; Dick, H.J.B.; Drouin, M. Pervasive melt percolation reactions in ultra-depleted refractory harzburgites at the Mid-Atlantic Ridge, 15° 20' N: ODP Hole 1274A. *Contrib. Mineral. Petrol.* **2007**, *153*, 303–319. [[CrossRef](#)]
67. Dick, H.J.B.; Fisher, R.L. Mineralogical studies of the residues of mantle melting: abyssal and alpine-type peridotites. In *Kimberlite II the Mantle and Crust-Mantle Relationships*; Kornprobst, J., Ed.; Elsevier: Amsterdam, The Netherlands, 1984; pp. 295–308.
68. Zhou, M.F.; Robinson, P.T.; Malpas, J.; Edwards, S.J.; Qi, L. REE and PGE geochemical constraints on the formation of dunites in the Luobusa Ophiolite, southern Tibet. *J. Petrol.* **2005**, *46*, 615–639. [[CrossRef](#)]
69. Uysal, I.; Ersoy, E.Y.; Dilek, Y.; Kapsiotis, A.; Sarifakioğlu, E. Multiple episodes of partial melting, depletion, metasomatism and enrichment processes recorded in the heterogeneous upper mantle sequence of the Neotethyan Eldivan ophiolite, Turkey. *Lithos* **2016**, *246–247*, 228–245. [[CrossRef](#)]
70. Hébert, R.; Adamson, A.C.; Komor, S.C. Metamorphic petrology of ODP 109, Hole 670A serpentinized peridotites: serpentinization processes at a slow spreading ridge environment. In *Proceedings of the ODP, Sci. Results 106/109*; Detrick, R., Honnorez, J., Bryan, W.B., Juteau, T., Eds.; 1990; pp. 103–115. Available online: http://www-odp.tamu.edu/publications/106109SR/VOLUME/CHAPTERS/sr106109_09.pdf (accessed on 17 February 2019).
71. Hellebrand, E.; Show, J.F.; Dick, H.J.B.; Hofmann, A.W. Coupled major and trace elements as indicators of the extent of melting in the mid-ocean-ridge peridotites. *Nature* **2001**, *410*, 677–681. [[CrossRef](#)] [[PubMed](#)]
72. Ishiwatari, A.; Sokolov, S.D.; Vysotskiy, S.V. Petrological diversity and origin of ophiolites in Japan and Far East Russia with emphasis on depleted harzburgite. *Geol. Soc. Lond. Spec. Publ.* **2003**, *218*, 597–617.s. [[CrossRef](#)]
73. Suhr, G.; Kelemen, P.; Paulick, H. Microstructures in Hole 1274A peridotites, ODP Leg 209, Mid-Atlantic Ridge: Tracking the fate of melts percolating in peridotite as the lithosphere is intercepted. *Geochem. Geophys. Geosyst.* **2008**, *9*. [[CrossRef](#)]
74. Seyler, M.; Toplis, M.J.; Lorand, J.P.; Luguët, A.; Cannat, M. Clinopyroxene microtextures reveal incompletely extracted melts in abyssal peridotites. *Geology* **2001**, *29*, 155–158. [[CrossRef](#)]
75. Hellebrand, E.; Snow, J.E.; Hoppe, P.; Hofmann, A.W. Garnet-field melting and late-stage refertilization in 'residual' abyssal peridotites from the Central Indian Ridge. *J. Petrol.* **2002**, *43*, 2305–2338. [[CrossRef](#)]
76. Brunelli, D.; Seyler, M.; Cipriano, A.; Ottolini, L.; Bonatti, E. Discontinuous melt extraction and weak refertilization of mantle Peridotites at the Vema Lithospheric Section (Mid-Antlantic Ridge). *J. Petrol.* **2006**, *47*, 745–771. [[CrossRef](#)]
77. Spiegelman, M.; Kelemen, P.B.; Aharonov, E. Causes and consequences of flow organization during melt transport: The Reaction infiltration instability. *J. Geophys. Res.* **2001**, *106*, 2061–2078. [[CrossRef](#)]
78. Matsumoto, I.; Arai, S. Morphological and chemical variations of chromian spinel in dunite-harzburgite complexes from the Sangun Zone (SW Japan): Implications for mantle/melt reaction and chromitite formation processes. *Mineral. Petrol.* **2001**, *73*, 305–323. [[CrossRef](#)]
79. Cannat, M.; Lagabrielle, Y.; Bougault, H.; Casev, J.; de Coutures, N.; Dmitriev, L.; Fouquet, Y. Ultramafic and gabbroic exposures at the Mid-Atlantic Ridge: geological mapping in the 15° N region. *Tectonophysics* **1997**, *279*, 193–213. [[CrossRef](#)]
80. Hellebrand, E.; Snow, J.; Dick, H.J.B.; Devey, C.W.; Hofmann, A.W. Reactive crack flow in the oceanic mantle: an ion probe study on cpx from vein-bearing abyssal peridotites. *Ophioliti* **1999**, *24*, 106–107.
81. Kaczmarek, M.A.; Müntener, O. Juxtaposition of melt impregnation and high-temperature shear zone in the mantle; Field and petrological constraints from the Lanzo peridotite (Northern Italy). *J. Petrol.* **2008**, *49*, 2187–2220. [[CrossRef](#)]
82. Zhang, P.; Uysal, I.; Zhou, M.; Su, B.; Avci, E. Subduction initiation for the formation of high-Cr chromitites in the kop ophiolite, NE Turkey. *Lithos* **2016**, *260*, 345–355. [[CrossRef](#)]
83. Batanova, V.G.; Sobolev, A.V. Compositional heterogeneity in subduction-related mantle peridotites, Troodos massif, Cyprus. *Geology* **2000**, *28*, 55–58. [[CrossRef](#)]
84. Parkinson, I.J.; Pearce, J.A.; Thirwall, M.F.; Johnson, K.T.M.; Ingram, G. Trace Element Geochemistry of Peridotites from the Izu-Bonin-Mariana forearc, Leg 125. Available online: http://www-odp.tamu.edu/publications/125_SR/VOLUME/CHAPTERS/sr125_28.pdf (accessed on 3 March 2017).
85. Smith, A.G. Tectonic significance of the Hellenic-Dinaric ophiolites. *Geol. Soc. Lond. Spec. Publ.* **1993**, *76*, 213–243. [[CrossRef](#)]

86. Bizimis, M.; Salters, V.J.M.; Bonatti, E. Trace and REE content of clinopyroxenes from supra-subduction zone peridotites. Implications for melting and enrichment processes in island arcs. *Chem. Geol.* **2000**, *165*, 67–85. [[CrossRef](#)]
87. Parkinson, I.J.; Pearce, J.A.; Thirwall, M.F.; Johnson, K.T.M.; Ingram, G. Trace element geochemistry of peridotites from the Izu-Bonin-Mariana forearc, Leg 125. In *Proceedings of the ODP science results, 125*. Ocean Drilling Program, College Station. Fryer, P., Pearce, J.A., Stokking, L.B., Eds.; 1992, pp. 487–506. Available online: <https://pdfs.semanticscholar.org/23cb/d23207c20eb9e2c1664d4a01a9b036da9bfa.pdf> (accessed on 17 February 2019).
88. Yang, J.S.; Robinson, P.T.; Dilek, Y. Diamonds in ophiolites. *Elements* **2014**, *10*, 127–130. [[CrossRef](#)]
89. Shervais, J.W. Birth, death, and resurrection: the life cycle of subduction zone ophiolites. *Geochem. Geophys.* **2001**, *2*, 1010. [[CrossRef](#)]



© 2019 by the authors. Licensee MDPI, Basel, Switzerland. This article is an open access article distributed under the terms and conditions of the Creative Commons Attribution (CC BY) license (<http://creativecommons.org/licenses/by/4.0/>).